



Fe–B–P–Cu nanocrystalline soft magnetic alloys with high B_s

Akiri Urata^{a,*}, Hiroyuki Matsumoto^a, Shigeyoshi Yoshida^a, Akihiro Makino^b

^a NEC TOKIN Corporation, 6-7-1 Koriyama, Taihaku-ku, Sendai, Miyagi 982-8510, Japan

^b Institute for Materials Research, Tohoku University, 2-1-1 Katahira Aoba-ku, Sendai, Miyagi 980-8577, Japan

ARTICLE INFO

Article history:

Received 1 July 2010

Received in revised form

14 December 2010

Accepted 15 December 2010

Available online 6 January 2011

Keywords:

Nanocrystalline alloy

High saturation magnetic flux density

Soft magnetic material

ABSTRACT

The effects of the addition of Cu on the crystallization processes, nanostructures and soft magnetic properties for the $\text{Fe}_{80.8-84.8}\text{B}_{8-10}\text{P}_{6-8}\text{Cu}_{1.2}$ alloys were investigated. The Fe–B–P–Cu alloys show two separated distinct exothermic peaks upon heating due to the addition of Cu. Furthermore, the interval temperature between each one for the $\text{Fe}_{82.8}\text{B}_9\text{P}_7\text{Cu}_{1.2}$ alloy is 103 K, and the first and second exothermic peaks result from the phase transition from amorphous to α -Fe and then to $\text{Fe}_3(\text{B,P})$, respectively. A uniform nanocrystalline structure composed of α -Fe grains with a 17 nm diameter was realized by annealing just above the first exothermic peak, and this nanocrystalline alloy exhibits high B_s of 1.70 T and low H_c of 4.9 A/m. Therefore, the nanocrystalline Fe–B–P–Cu soft magnetic alloy with high B_s and low H_c has a large industrial advantage due to miniaturization, high efficiency and low material cost of electric devices.

© 2010 Elsevier B.V. All rights reserved.

1. Introduction

Recently, soft magnetic materials with high characteristics are very much required to achieve miniaturization and high efficiency of electric devices. We have already reported that the replacement of Fe by Nb is effective for the enhancement of the glass forming ability in a Fe–B–P system, and that Fe–B–P–Nb glassy alloy shows excellent soft magnetic properties compared with commercial alloys [1–3]. However this alloy has relatively low saturation magnetic flux density (B_s) of 1.2–1.3 T for the addition of Nb element and large saturation magnetostriction (λ_s) of 17×10^{-6} . On the other hand, nanocrystalline alloys such as Fe–Si–B–Nb–Cu [4,5] and Fe–B–Nb [6,7] have low coercivity (H_c) and high permeability (μ) due to zero λ_s . Moreover, nanocrystalline Fe–Si–B–Cu [8,9] and Fe–Si–B–P–Cu [10–13] alloys exhibit high B_s and low H_c due to high Fe content and no Nb. We report in this study about the $\text{Fe}_{80.8-84.8}\text{B}_{8-10}\text{P}_{6-8}\text{Cu}_{1.2}$ nanocrystalline alloys with high B_s and low H_c , which have been achieved by choosing Nb-free chemical compositions with both Cu addition for enhancing nanocrystallization and high Fe content.

2. Experimental

Fe–B–P–(Nb, Cu) alloy ingots were prepared by high frequency induction heating method in an Ar atmosphere. A single-roller melt-spinning method in air was used to produce rapidly solidified ribbons, 15 mm in width and about 20 μm in thickness. Thermal stability was evaluated with a differential scanning calorimeter (DSC) at a heating rate of 0.67 K/s under an Ar flow. The as-quenched and annealed structures

were examined by X-ray diffraction (XRD) with Cu $K\alpha$ radiation and transmission electron microscopy (TEM). The melt-spun ribbons were subjected to annealing for 600 s at various temperatures under an Ar flow. B_s under a maximum applied field of 800 kA/m was measured by a vibrating sample magnetometer (VSM). H_c under a maximum applied field of 2–4 kA/m was measured by a DC–BH loop tracer using a single sheet. The saturation magnetostriction (λ_s) was measured by using a strain gage method.

3. Results and discussion

The effects of replacement of Fe by Cu and metalloid elements such as B, P by Fe on the crystallization process of Fe–B–P–Cu alloys were investigated. Fig. 1 shows the DSC curves for the as-quenched $\text{Fe}_{80.8}\text{B}_{10}\text{P}_8\text{Cu}_{1.2}$, $\text{Fe}_{82.8}\text{B}_9\text{P}_7\text{Cu}_{1.2}$ and $\text{Fe}_{84.8}\text{B}_8\text{P}_6\text{Cu}_{1.2}$ alloy ribbons, together with the data of the $\text{Fe}_{82}\text{B}_{10}\text{P}_8$ and $\text{Fe}_{78}\text{B}_{10}\text{P}_8\text{Nb}_4$ alloy ribbons. The $\text{Fe}_{82}\text{B}_{10}\text{P}_8$ alloy ribbon shows a sharp exothermic peak and the $\text{Fe}_{78}\text{B}_{10}\text{P}_8\text{Nb}_4$ alloy ribbon shows the glass transition, followed by a supercooled liquid region and high glass-forming ability [1–3]. On the other hand, the Fe–B–P–Cu alloy ribbons show two separated distinct exothermic peaks upon heating, and temperature intervals between each one are 73 K, 103 K and 123 K, respectively. Fig. 2 shows the XRD patterns of the $\text{Fe}_{82.8}\text{B}_9\text{P}_7\text{Cu}_{1.2}$ ribbons at the annealing temperature of 698 and 748 K, together with the XRD pattern of the as-quenched ribbon for comparison. The as-quenched ribbon consists only of a broad peak, and no peaks corresponding to crystalline phase. The XRD pattern of the ribbon annealed at 698 K is identified as an α -Fe phase, and the XRD pattern of the ribbon annealed at 748 K is identified as mixed phases of α -Fe and $\text{Fe}_3(\text{B,P})$. Therefore, it is considered that the first and second exothermic peaks are attributed to the precipitation of the α -Fe and $\text{Fe}_3(\text{B,P})$ phases, respectively, and the one

* Corresponding author.

E-mail address: a-urata@wh.jp.nec.com (A. Urata).

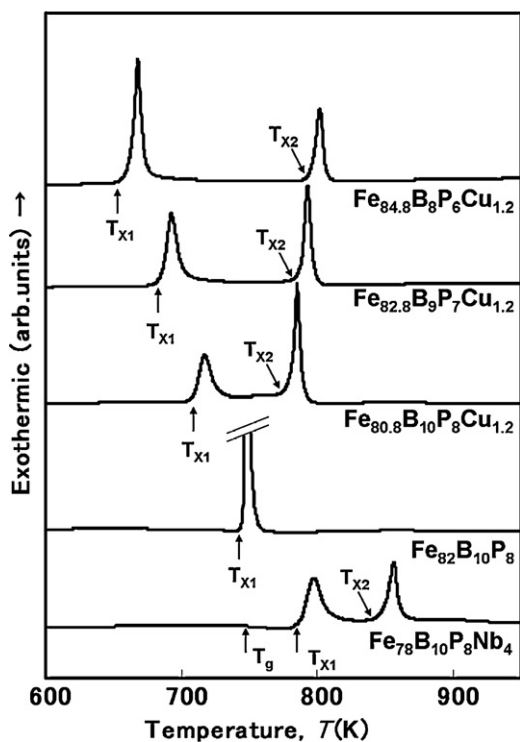


Fig. 1. The DSC curves of the as-quenched Fe–B–P–Cu alloys. The data of $\text{Fe}_{82}\text{B}_{10}\text{P}_8$ and $\text{Fe}_{78}\text{B}_{10}\text{P}_8\text{Nb}_4$ alloys are also shown for comparison.

peak of the ternary alloy corresponds to the precipitation of the two phases.

Fig. 3 shows the H_c of $\text{Fe}_{82}\text{B}_{10}\text{P}_8$ and Fe–B–P–Cu alloys as a function of annealing temperature. H_c of the $\text{Fe}_{82}\text{B}_{10}\text{P}_8$ alloy increases rapidly in the temperature range above 698 K. On the other hand, H_c of the Fe–B–P–Cu alloys exhibit lower H_c in the temperature range

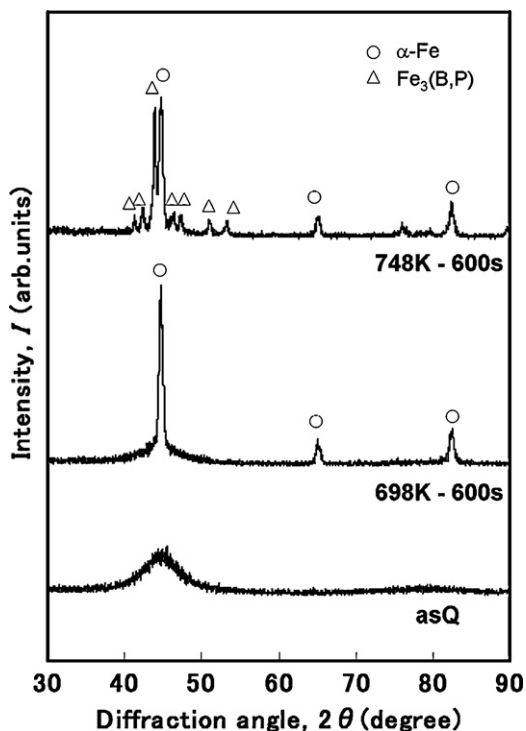


Fig. 2. The XRD patterns of the as-quenched and annealed $\text{Fe}_{82.8}\text{B}_9\text{P}_7\text{Cu}_{1.2}$ ribbons.

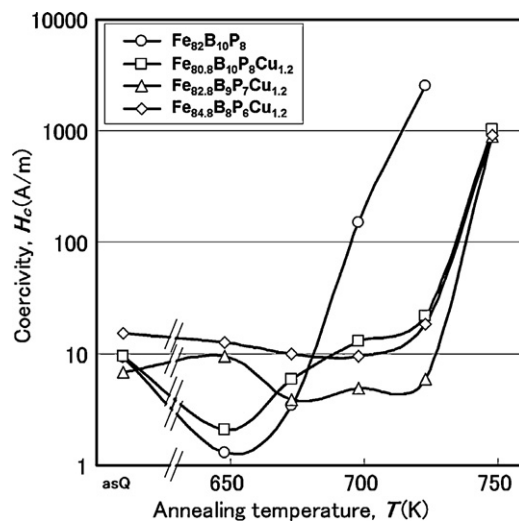


Fig. 3. The H_c of Fe–B–P–Cu alloys as a function of annealing temperature.

of 648–723 K and H_c annealed just above the first exothermic peak are 22.1, 4.9 and 9.4 A/m, respectively.

Fig. 4 shows the TEM images of the (a) as-quenched and (b) crystallized $\text{Fe}_{82.8}\text{B}_9\text{P}_7\text{Cu}_{1.2}$ alloy ribbons. The TEM image indicates that the as-quenched alloy ribbon has a single amorphous structure. On the other hand, Fig. 4(b) shows a homogeneous nanostructure composed of grains 17 nm in diameter, because of an unusual effect of the simultaneous addition of P and Cu [10–13]. In addition,

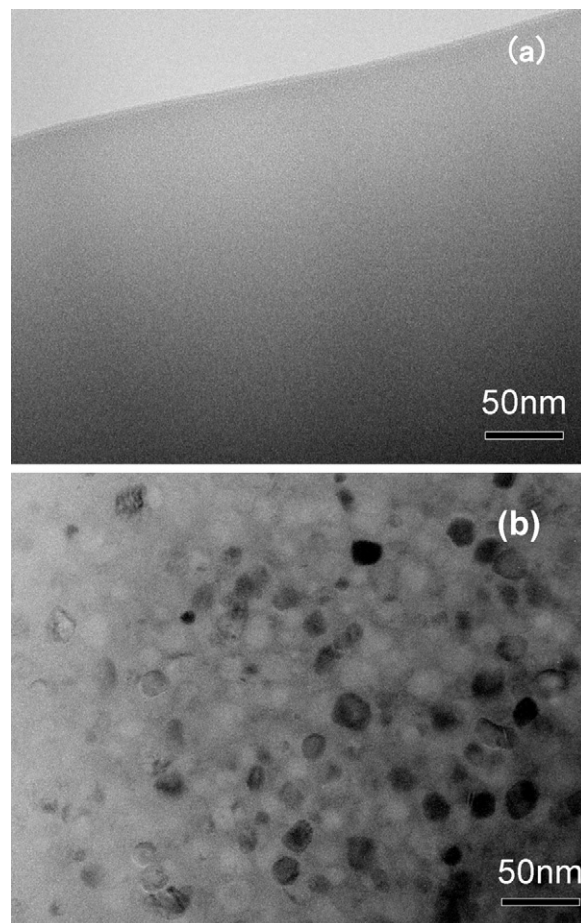
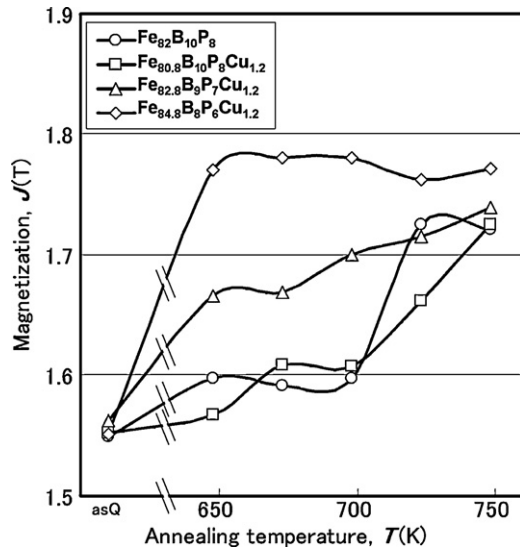


Fig. 4. TEM images of (a) as-quenched and (b) crystallized $\text{Fe}_{82.8}\text{B}_9\text{P}_7\text{Cu}_{1.2}$ alloys.

Table 1

Thermal stability and magnetic properties of the Fe–B–P–Cu alloys. The data of the Fe–B–P and Fe–B–P–Nb alloys are also shown for comparison.

	As-quenched				Crystallized			
	T_{x1} (K)	T_{x2} (K)	ΔT_x (K)	H_c (A/m)	B_s (T)	H_c (A/m)	B_s (T)	Annealing condition
Fe _{80.8} B ₁₀ P ₈ Cu _{1.2}	709	782	73	9.5	1.55	22.1	1.66	723 K × 10 min
Fe _{82.8} B ₉ P ₇ Cu _{1.2}	686	789	103	6.8	1.56	4.9	1.70	698 K × 10 min
Fe _{84.8} B ₈ P ₆ Cu _{1.2}	663	796	123	15.4	1.55	9.4	1.78	698 K × 10 min
Fe ₈₂ B ₁₀ P ₈	745	–	–	9.3	1.55	2460	1.72	748 K × 10 min
Fe ₇₈ B ₁₀ P ₈ Nb ₄	786	846	60	17.9	1.24	920	1.30	798 K × 10 min

**Fig. 5.** The B_s of Fe–B–P–Cu alloys as a function of annealing temperature.

tion, the λ_s is 14×10^{-6} , which is a smaller value than that of the Fe–B–P–Nb glassy alloy and Fe-based amorphous alloy due to competition of negative and positive magnetostrictions generated in the α -Fe grains and the amorphous phase, respectively [14]. As a result, the crystallized Fe_{82.8}B₉P₇Cu_{1.2} alloy exhibits low H_c because of homogeneous nanostructure composed of α -Fe with low λ_s .

Fig. 5 shows the B_s of Fe₈₂B₁₀P₈ and Fe–B–P–Cu alloys as a function of annealing temperature. B_s of the alloys increases with increasing annealing temperature because of a structural change from the amorphous phase to the nanocrystalline phase. Furthermore, the Fe-rich Fe_{82.8}B₉P₇Cu_{1.2} and Fe_{84.8}B₈P₆Cu_{1.2} alloys annealed at 698 K exhibit high B_s of 1.70 and 1.78 T, respectively.

Table 1 summarizes the thermal stability and magnetic properties of the Fe–B–P–Cu alloys. The data of the Fe–B–P and Fe–B–P–Nb alloys are also shown for comparison. The Cu added alloys crystallize through two exothermic peaks, and the temperature intervals between each one extend with increasing Fe content. The H_c of Cu-free alloys largely increases after annealing due to the grain growth and precipitated compound phase. On the other hand, the annealed

Fe_{82.8}B₉P₇Cu_{1.2} and Fe_{84.8}B₈P₆Cu_{1.2} alloys exhibit simultaneously high B_s and low H_c . Therefore, the nanocrystalline Fe–B–P–Cu alloys have advantages as industrial magnetic materials and are expected to be used for energy saving of electric devices.

4. Conclusions

The crystallization processes, nanostructures and soft magnetic properties of the Fe–B–P–Cu alloys have been investigated and we have successfully developed a Fe–B–P–Cu nanocrystalline alloy with combination of high B_s and low H_c . The results obtained are summarized as follows.

- (1) Fe_{80.8}B₁₀P₈Cu_{1.2}, Fe_{82.8}B₉P₇Cu_{1.2} and Fe_{84.8}B₈P₆Cu_{1.2} alloy ribbons show two separated distinct exothermic peaks, the temperature intervals between each one are 73 K, 103 K and 123 K, respectively, and the first and second exothermic peaks are attributed to the precipitation of the α -Fe and Fe₃(B,P) phases, respectively.
- (2) The crystallized Fe_{82.8}B₉P₇Cu_{1.2} alloy annealed at 698 K exhibits a uniform and fine structure composed of α -Fe grains with 17 nm in diameter.
- (3) The nanocrystalline Fe_{82.8}B₉P₇Cu_{1.2} alloy exhibits good soft magnetic properties such as a high B_s of 1.70 T and low H_c of 4.9 A/m.

References

- [1] H. Matsumoto, A. Urata, Y. Yamada, A. Makino, Dig. Intermag. CF-10 (2008).
- [2] H. Matsumoto, A. Urata, Y. Yamada, A. Makino, J. Appl. Phys. 105 (2009) 07A317.
- [3] H. Matsumoto, A. Urata, Y. Yamada, A. Inoue, IEEE Trans. Mag. 46 (2010) 373.
- [4] Y. Yoshizawa, S. Oguma, K. Yamauchi, J. Appl. Phys. 64 (1988) 6044.
- [5] Y. Yoshizawa, K. Yamauchi, J. Jpn. Inst. Met. 53 (1989) 241.
- [6] K. Suzuki, N. Kataoka, A. Inoue, A. Makino, T. Masumoto, Mater. Trans. JIM 31 (1990) 743.
- [7] A. Makino, K. Suzuki, A. Inoue, T. Masumoto, Mater. Trans. JIM 32 (1991) 551.
- [8] M. Ohta, Y. Yoshizawa, J. Phys. Lett. 91 (2007) 062517.
- [9] M. Ohta, Y. Yoshizawa, J. Appl. Phys. 103 (2008) 07E722.
- [10] A. Makino, H. Men, T. Kubota, K. Yubuta, A. Inoue, Mater. Trans. 50 (2009) 204.
- [11] A. Makino, H. Men, T. Kubota, K. Yubuta, A. Inoue, J. Appl. Phys. 105 (2009) 07A308.
- [12] A. Makino, H. Men, T. Kubota, K. Yubuta, A. Inoue, IEEE Trans. Mag. 45 (2009) 4302.
- [13] L. Cui, H. Men, A. Makino, T. Kubota, K. Yubuta, M. Qi, A. Inoue, Mater. Trans. 50 (2009) 2515.
- [14] G. Herzer, Mater. Sci. Eng. A 133 (1991) 1.